THE ROYAL SOCIETY

Aspects of solid propellant combustion

By C. A. Lowe[1] and J. F. Clarke[2]

[1]*Department of Applied Mathematics and Theoretical Physics, University of Cambridge, Silver Street, Cambridge CB3 9EW, UK*
[2]*College of Aeronautics, Cranfield University, Cranfield, Bedfordshire MK43 0AL, UK*

Internal ballistics describes the combustion of solid propellant within a closed combustion chamber. This is achieved by modelling a mixture of incompressible solid particles and compressible reactive gases with averaged equations of two-phase flow. The combustion of the solid is described with interaction terms that define the rate of mass, momentum and energy exchange from solid into gas. This work concentrates on modelling ignition and the initial stages of combustion, proposing the concept of 'gaseous ignition' by including time-scales of chemical reaction in the gas phase. These non-equilibrium effects are placed firmly within the context of internal ballistics by making direct comparisons between experimental pressure-time histories. In particular, excellent agreement can be achieved between numerical simulations and experimental work by assuming a two-stage reaction process during which the rate of chemical energy release will significantly differ from a single exothermic reaction.

Keywords: non-equilibrium flow; ignition; multiphase flow; internal ballistics; shock-capturing methods

1. Introduction

Internal ballistics modelling involves the combustion of highly energetic propellant materials. Propellants burn rapidly, releasing large quantities of chemical energy, which explains their use as the fuel that powers rocket motors and ballistic weapons. Traditionally, propellant has been used in solid form—such as granular or stick form—and this work will focus on the combustion of these types.

Early theoretical work on internal ballistics was primarily concerned with calculation of the exit velocity of the projectile. The force on the projectile is predicted by calculating the pressure history at the projectile base, from which the acceleration and projectile velocity can be deduced. The methodology is well documented in the book by Corner (Great Britain Ministry of Supply Scientific Advisory Council 1951). The first models proved to be moderately accurate at calculating muzzle velocities and peak pressure, but no serious attempt was made to include flow dynamics in the chamber and the problem was regarded as a 'well-stirred' or 'lumped parameter' system. Vielle's law of burning was recognized at this time, which provides a formula for the rate of regression of the solid propellant surface $\dot{r}$ as a function of external gas pressure and a number of empirical constants specific to each propellant type. In addition, effort was devoted towards constructing formulae that would provide the rate of change of burning surface area over time for quite complicated propellant geometries. A reasonable assumption to make is that the exposed area of any

propellant shape will regress evenly subject to some uniform external pressure and temperature, described as 'parallel burning'. From this the idea of the form function was constructed by Corner—detailed in Great Britain Ministry of Supply Scientific Advisory Council (1951)—which provides a relationship between the rate of burning $\dot{r}$ and the exposed surface area S_{p}. The combination of these two ideas produces a method of measuring the rate of mass transfer from solid to gas:

$$\dot{m} = \rho_{\mathrm{p}} S_{\mathrm{p}} \dot{r}, \tag{1.1}$$

where $\dot{m}$ (kg m^{-3} s^{-1}) is the rate of gaseous mass addition and ρ_{p} (kg m^{-3}) is the density of the solid propellant. Along with this, an experimentally derived energy of combustion is taken for the propellant Q (J kg^{-1}) and the rate of energy and pressure increase in the gas phase can be deduced. During these studies, it was soon apparent that at high pressures the reactant gas could not be described accurately using the ideal gas equation and a covolume equation was adopted. Both Vielle's law and Corner's theory are key elements in internal ballistics modelling today.

These simple ideas were soon extended to one dimension and it was quickly apparent that not only did the gas dynamics need to be considered but also the solid-particle motion. From these beginnings sprung the multidimensional multiphase models that are employed today in internal ballistic codes. Final solutions are obtained using a combination of high-speed computers and advanced numerical methods.

However, despite these advances that are centred around the action of modern day computer facilities, some of the dominant physical mechanisms of the combustion cycle have been overlooked, in particular ignition. Ignition modelling has been quite crude in many internal ballistics codes. Many assumed that once the gas temperature increases above some experimentally measured 'ignition temperature', then the propellant grain would burn at a rate governed by Vielle's law. The weakness of the ignition temperature idea is that it is supposed to encompass all of the intricate heat-transfer processes between the gas and solid, solid thermochemistry, solid-phase reactions and gas-phase reactions. A slight improvement to this involved the solution of a heat-conduction problem between the gas and solid-surface as described in Peretz *et al*. (1973). In this case ignition is deemed to occur once the solid surface attains some empirically derived temperature after which combustion continues according to Vielle's law. Both of these theories do not explain how experiments can measure distinct time differences between first gasification followed by ignition.

As summarized in the comprehensive review of solid propellant ignition modelling by Hermance (1984), ignition is controlled by a gas-phase reaction that is directly influenced by solid-surface reactions. A model that includes gas-phase reaction to describe the ignition process and supporting numerical methods has already been described in Clarke & Lowe (1996) and Lowe *et al*. (1995). These ideas were developed in Lowe (1996) to include a pyrolysis reaction at the solid surface dependent on surface temperature. In this work the very simple chemical gas-phase regime assumed in Clarke & Lowe (1996) will be built upon to produce chemical schemes closer to the known reactions that occur during propellant combustion. These chemical schemes will be included in the one-dimensional two-phase flow equations. To test the effect of the various reactions, two simulations will be illustrated: the first is a test problem for which the early ignition phase of the combustible two-phase will be analysed.

The second simulates the entire combustion cycle and comparisons are made with experimental data.

The configuration of an internal ballistic combustion chamber involves a combustion chamber that is almost cylindrical, although some tapering occurs at either end. This contains solid propellant granules, which are assumed to be evenly dispersed in the chamber volume (the effect of gravity is neglected). A perforated tube is located along part of the axial length through which a hot inert 'igniter' gas is vented at a prescribed rate $\dot{m}_{\mathrm{ig}}$ (kg m^{-3} s^{-1}). Heat transfer between the hot igniter gases and solid granules raises the temperature of the solid-propellant surface. Subsequently, the solid will gasify, producing a source of hot reactant gas that will increase the pressure in the chamber. A projectile, positioned at one extreme of the chamber, begins to move once some critical pressure has been attained at the projectile base. As the projectile moves down the barrel of the weapon, resistive forces are transmitted between the barrel wall and the projectile. This is at least a two-dimensional problem; however, primarily it is the average pressure at any axial length that is of interest and so for simplicity the quasi-one-dimensional† configuration will be assumed whereby the sources of igniter gas are evenly distributed over the cross-sectional area.

The modelling of the combustion cycle described above is achieved through the solution of average two-phase flow equations. The phases involved are the incompressible solid particles and the compressible reactive gases of combustion. The equations as originally derived by Gough (1974) are

$$\frac{\partial}{\partial t}(\rho\epsilon) + \frac{\partial}{\partial x}(\rho\epsilon u) = \dot{m} + \dot{m}_{\mathrm{ig}}, \tag{1.2}$$

$$\frac{\partial}{\partial t}(\rho\epsilon u) + \frac{\partial}{\partial x}(\epsilon(\rho u^2 + p)) = p\frac{\partial \epsilon}{\partial x} + \dot{m}u_{\mathrm{p}} - D, \tag{1.3}$$

$$\frac{\partial}{\partial t}(\epsilon E) + \frac{\partial}{\partial x}(\epsilon u(E+p)) = \dot{m}(Q + \kappa_{\mathrm{p}}) + \dot{m}_{\mathrm{ig}}Q_{\mathrm{ig}} - p\frac{\partial(1-\epsilon)(u_{\mathrm{p}})}{\partial x} - u_{\mathrm{p}}D - q_{\mathrm{loss}}, \tag{1.4}$$

$$\frac{\partial}{\partial t}(\rho_{\mathrm{p}}(1-\epsilon)) + \frac{\partial}{\partial x}(\rho_{\mathrm{p}}(1-\epsilon)u_{\mathrm{p}}) = -\dot{m}, \tag{1.5}$$

$$\frac{\partial}{\partial t}(\rho_{\mathrm{p}}(1-\epsilon)u_{\mathrm{p}}) + \frac{\partial}{\partial x}((1-\epsilon)(\rho_{\mathrm{p}}{u_{\mathrm{p}}}^2 + p_{\mathrm{int}})) = -(1-\epsilon)\frac{\partial p}{\partial x} - \dot{m}u_{\mathrm{p}} + D, \tag{1.6}$$

$$\frac{\partial}{\partial t}(N) + \frac{\partial}{\partial x}(Nu_{\mathrm{p}}) = 0; \tag{1.7}$$

where ϵ is the porosity (volume fraction occupied by the gas), u is the gas velocity, u_{p} is the particle velocity, p is the gas pressure, $\kappa_{\mathrm{p}} = \frac{1}{2}u_{\mathrm{p}}^2$ is the kinetic energy of the particles, D is the viscous drag, p_{int} is the intergranular stress and N is the number of solid particles. Fragmentation or coalescence of the particles is not assumed to occur. Q is the energy of formation of the propellant and Q_{ig} is the energy of formation of the igniter. The total energy E of the gas was defined in Gough's model as

$$E = \rho(e + \kappa), \tag{1.8}$$

† Includes small changes of cross-sectional area in a quasi-one-dimensional manner.

where e is the thermal energy and $\kappa = \frac{1}{2}u^2$. A covolume equation of state is considered to hold for the gas:

$$e = \frac{p(1 - b\rho)}{\rho(\gamma - 1)}, \tag{1.9}$$

where p is the gas pressure, b (m kg^{-3}) is the covolume and γ is the ratio of specific heats. During the solution of the solid-momentum equation, the buoyancy force on the solid-particle movement is assumed to be negligible. The viscous drag between the gas and the solid will alone control the particle movement. Omitting the pressure gradient term has been chosen as a physically plausible way of removing ill-posedness from the system where the intergranular stress is non-zero. The ill-posedness has been recognized by many previous authors (Drew 1983; Ransom & Hicks 1984) to be an undesirable feature of the incompressible two-phase flow equations and the neglect of buoyancy forces has been suggested (Soo 1979; Smirnov & Dimitrenko 1992). Empirical relations for the drag and intergranular stress are detailed in Lowe (1996).

2. Multiple reactions

The intention is to incorporate time-scales associated with chemical times of a series of general gas-phase reactions that are occurring during propellant combustion.

Assuming that any solid or surface reactions are thermally neutral, then the conservation of species' mass and energy can be rewritten as follows:

$$\frac{\partial}{\partial t}(\rho c_\alpha \epsilon) + \frac{\partial}{\partial x}(\rho \epsilon u c_\alpha) = \dot{m}_\alpha + K_\alpha, \quad \alpha = 1, \ldots, n, \tag{2.1}$$

$$\frac{\partial}{\partial t}(\epsilon E) + \frac{\partial}{\partial x}(\epsilon u(E + p)) = (\dot{m} + \dot{m}_{\mathrm{ig}})(e_{\mathrm{th}} + pv) + \sum_{\alpha=1}^{n} \dot{m}_\alpha Q_\alpha - \dot{m}L + \dot{m}_{\mathrm{ig}} Q'_{\mathrm{ig}} - p\frac{\partial(1 - \epsilon)(u_{\mathrm{p}})}{\partial x} - u_{\mathrm{p}} D - q_{\mathrm{loss}}, \tag{2.2}$$

where c_α is the mass fraction of species α in the gas phase. In general,

$$E \equiv \sum_{\alpha=1}^{n} [c_\alpha (e_\alpha(T) + Q_\alpha)] + \kappa, \tag{2.3}$$

where $e_\alpha(T)$ is the thermal energy of species α, assumed to depend only upon the local absolute temperature T, and Q_α is the specific energy of formation of that species. Note that $\dot{m}$ is formally made up from contributions from all of the species, so that one can write

$$\dot{m} = \sum_{\alpha=1}^{n} \dot{m}_\alpha. \tag{2.4}$$

For simplicity it will be assumed that $e_\alpha = e \forall \alpha$. It is assumed that, to gasify the solid propellant, L units of energy per unit mass of propellant may need to be supplied from the gas phase. The chemical kinetics of the possible controlling reaction in the combustion process will be discussed in a little more detail below. However, before this the main differences between the energy equations (1.4) and (2.2) will be described.

(*a*) *Conditions at the gas–solid interface*

Of particular significance are the very different source terms that appear on the right-hand side of the energy equations (1.4) and (2.2). These source terms represent the addition of energy into the closed volume due to the combustion of the propellant material and igniter gas. Equation (1.4) describes how the solid will gasify at rate $\dot{m}$ and the corresponding energy of formation of the *solid* is given as Q. Thus, this actually represents the rate of energy loss from the solid propellant. Similarly, all energy increase due to the combustion of hot igniter gas is described by the term $\dot{m}_{\mathrm{ig}}Q_{\mathrm{ig}}$.

The source term in equation (2.2) describes the increase in energy in the gas phase due to propellant combustion—rather than the decrease of energy in the solid. Along with this it also distinguishes between the energy increase due to the addition of a gas into a closed system, irrespective of whether it is a reactive gas or not, and energy increase due to gas-phase chemical reaction. The former of these contributions from both the propellant and igniter gases is $(\dot{m}+\dot{m}_{\mathrm{ig}})(e_{\mathrm{th}}+pv)$ and the latter is given as $\sum_{\alpha=1}^{n}\dot{m}_\alpha Q_\alpha+\dot{m}_{\mathrm{ig}}Q'_{\mathrm{ig}}$, where Q_α is the energy of formation of the various α gas-phase reactants and Q'_{ig} is the *chemical* energy of the igniter gas. Finally, the term $\dot{m}L$ represents latent heat requirements to gasify the solid propellant material. For the source terms in equations (1.4) and (2.2) to be equal the following equivalences *must* hold at the interface:

$$\dot{m}(e_{\mathrm{th}}+pv)+\sum_{\alpha=1}^{n}\dot{m}_\alpha Q_\alpha-\dot{m}L\equiv\dot{m}(Q+\kappa_{\mathrm{p}}),\tag{2.5}$$

$$\dot{m}_{\mathrm{ig}}(e_{\mathrm{th}}+pv)+\dot{m}_{\mathrm{ig}}Q'_{\mathrm{ig}}\equiv\dot{m}_{\mathrm{ig}}(Q_{\mathrm{ig}}+\kappa_{\mathrm{ig}}).\tag{2.6}$$

The kinetic energy of the igniter κ_{ig} is assumed to be negligible in this study.

(*b*) *One-step reaction*

Assume that the propellant $R(s)$ gasifies and produces reactant gases that are controlled by a single irreversible reaction

$$R(s)\xrightarrow{\dot{m}}X(g)+F(g)\xrightarrow{\Omega}2P(g),\tag{2.7}$$

where $F(g)$ is a fuel, $X(g)$ is an oxidizer and $P(g)$ is an inert product gas. If the molecular weights of the three species are assumed to be the same and equal to W, then the reaction rates are

$$K_X=K=-\rho\Omega c_X c_F,\quad K_F=K=-\rho\Omega c_X c_F,\quad K_P=-2K=2\rho\Omega c_X c_F,\tag{2.8}$$

where Ω (s^{-1}) is the chemical frequency, which can be given as

$$\Omega=A_{\mathrm{g}}p\exp(-E_{\mathrm{A}}/\mathcal{R}T).\tag{2.9}$$

Here $(A_{\mathrm{g}}p)$ is the frequency of binary collisions in the gas phase and E_{A} is the activation energy. Furthermore, it is assumed that the mass that is introduced into the system is half composed of X and the other half is F, so that $\dot{m}_X=\dot{m}_F=\frac{1}{2}\dot{m}$. Using the simplifications described above, the mass-fraction equation (2.1), where $\alpha=X,F$, gives

$$\frac{\partial(\rho\epsilon c_\alpha)}{\partial t}+\frac{\partial(\rho\epsilon u c_\alpha)}{\partial x}=K+\tfrac{1}{2}\dot{m}.\tag{2.10}$$

These species equations for fuel and oxidant, equation (2.10) for $\alpha = F$ and X, respectively, can be subtracted, and substituting the mass equation (1.2) into this difference provides the relation

$$(\dot{m} + \dot{m}_{\mathrm{ig}})(c_F - c_X) + \rho\epsilon \frac{\mathrm{D}(c_F - c_X)}{\mathrm{D}t} = 0. \tag{2.11}$$

Equation (2.11) can be integrated formally to give

$$(c_F - c_X) = (c_F - c_X)_0 \exp\left(\int_0^t \frac{(\dot{m} + \dot{m}_{\mathrm{ig}})}{\rho\epsilon} \partial t \right). \tag{2.12}$$

One possible solution of this is to make $c_X = c_F \equiv c$, which will be done here, and the above equations for the species can be reduced to only one species equation that applies to both X and F, namely

$$\frac{\partial(\rho\epsilon c)}{\partial t} + \frac{\partial(\rho\epsilon u c)}{\partial x} = \tfrac{1}{2}\dot{m} - \rho\Omega c^2. \tag{2.13}$$

Substitution of the interface conditions defined in equations (2.5) and (2.6) into the source terms of the energy equation (2.2) defines the following energy equation that includes the evolution of a gas-phase reactant:

$$\frac{\partial}{\partial t}(\epsilon E) + \frac{\partial}{\partial x}(\epsilon u(E + p)) = -p\frac{\partial(1-\epsilon)u_{\mathrm{p}}}{\partial x} + \dot{m}(Q + \kappa_{\mathrm{p}}) + \dot{m}_{\mathrm{ig}} Q_{\mathrm{ig}} - u_{\mathrm{p}} D - q_{\mathrm{loss}}, \tag{2.14}$$

where now the total energy is redefined from equation (2.3) as

$$E = \rho(e + \kappa + 2cQ_{\mathrm{g}}). \tag{2.15}$$

(c) *Two-step reaction*

Now assume that a reduced chemical scheme for the burning of solid propellant $R(s)$ can be summarized by the following sequence of reactions:

$$R(s) \xrightarrow{\dot{m}} R(g) \xrightarrow{\Omega_{\mathrm{R}}} F(g) + X(g) \xrightarrow{\Omega} 2P(g). \tag{2.16}$$

The solid propellant $R(s)$ is gasified at the rate $\dot{m}$ and converted into $R(g)$, which has an energy of formation Q_{R}. The latter reactant is broken down into gaseous fuel and oxidizer species F and X, which again have energies of formation Q_{g}, in a rapid (highly localized) reaction, whose chemical frequency, or inverse chemical time, is given by Ω_{R}; X and F react at a local rate, controlled by the frequency Ω, to form product species P whose energy of formation is zero. Use of the assumption of equal molecular weights for $X(g)$ and $F(g)$ and assuming that the product gas of the first reaction is half composed of X and F, it is clear that

$$K_{\mathrm{R}} = -\rho\Omega_{\mathrm{R}} c_{\mathrm{R}}, \quad K_F \equiv K_X = \tfrac{1}{2}\rho\Omega_{\mathrm{R}} c_{\mathrm{R}} - \rho\Omega c^2 = -\tfrac{1}{2}K_{\mathrm{R}} + K. \tag{2.17}$$

The governing equations can then be derived from equations (2.1), (2.2) as (mass-fraction equations are defined for reactant R and X or F)

$$\frac{\partial}{\partial t}(\rho\epsilon c_{\mathrm{R}}) + \frac{\partial}{\partial x}(\rho\epsilon c_{\mathrm{R}} u) = \dot{m} + K_{\mathrm{R}}, \tag{2.18}$$

$$\frac{\partial}{\partial t}(\rho\epsilon c) + \frac{\partial}{\partial x}(\rho\epsilon c u) = -\tfrac{1}{2}K_{\mathrm{R}} + K, \tag{2.19}$$

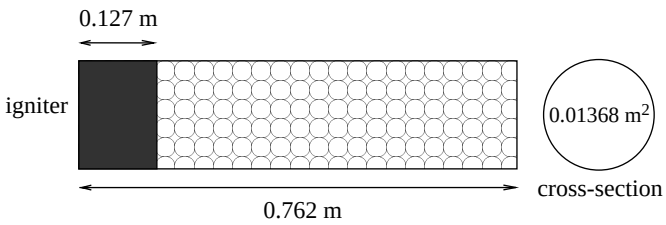

Figure 1. The one-dimensional combustion chamber.

the energy equation is (2.14) and the total energy is defined as

$$E = \rho(e + \kappa + 2cQ_{\mathrm{g}} + c_{\mathrm{R}}Q_{\mathrm{R}}). \tag{2.20}$$

(*d*) *Fast reactions*

In this section the relationship between the simple equilibrium model and the models that include finite-rate gas-phase chemical reactions will be explored. It is clear that the models must be equivalent under some limiting conditions, namely when gas-phase chemical times approach zero, implying that the chemical frequency must tend to infinity.

If the one-step reaction is such a fast reaction, then to remain physically meaningful for $\Omega \to \infty$, K must remain bounded. In this case $c \to 0$ and consequently $\mathrm{D}c/\mathrm{D}t \to 0$. Substitution into equation (2.13) implies that $K \to \frac{1}{2}\dot{m}$, which on substitution into the energy equation (2.15) shows how the non-equilibrium governing equations tend to the equilibrium system described in equations (1.2)–(1.8).

The same arguments can be applied to the two-step system: in this case for the first reaction to be infinitely fast it follows that $c_{\mathrm{R}} \to 0$ and $\mathrm{D}c_{\mathrm{R}}/\mathrm{D}t \to 0$. This implies that $K_{\mathrm{R}} \to \dot{m}$ and using the equivalent arguments for the second step $K \to \frac{1}{2}K_{\mathrm{R}} \to \frac{1}{2}\dot{m}$. Again by making these assumptions the equations will revert back to the equilibrium system.

For these investigations let us assume that the single-step reaction and the second part of the two-step reaction are *not* infinitely fast. However, if the first stage of the two-step reaction is in equilibrium, then all energy release associated with this reaction occurs instantaneously on gasification and the solution of equation (2.18) will not be necessary (since this occurs infinitely fast).

3. Numerical methods

The numerical method used to solve the two-phase system, equations (1.2)–(1.7), along with species equation (2.13) will now be outlined.

The system of partial differential equations can be written in the form

$$\boldsymbol{U}_t + \boldsymbol{F}(\boldsymbol{U})_x = \boldsymbol{S}(\boldsymbol{U}), \tag{3.1}$$

where $\boldsymbol{U}$, the vector of conserved variables, is given by

$$\boldsymbol{U} = (\boldsymbol{U}_{\mathrm{g}}, \boldsymbol{U}_{\mathrm{p}})^{\mathrm{T}}, \quad \text{where } \boldsymbol{U}_{\mathrm{g}} = (\rho, \rho c, \rho u, E)^{\mathrm{T}}, \quad \boldsymbol{U}_{\mathrm{p}} = (\rho_{\mathrm{p}}, \rho_{\mathrm{p}} u_{\mathrm{p}}, N)^{\mathrm{T}} \tag{3.2}$$

and the flux and source terms, $\boldsymbol{F}(\boldsymbol{U})$ and $\boldsymbol{S}(\boldsymbol{U})$, are functions of $\boldsymbol{U}$.

The method of fractional steps (Yanenko 1977) is used to split the problem, as originally suggested by Toro (1989*a*), into subproblems so that the flow equations

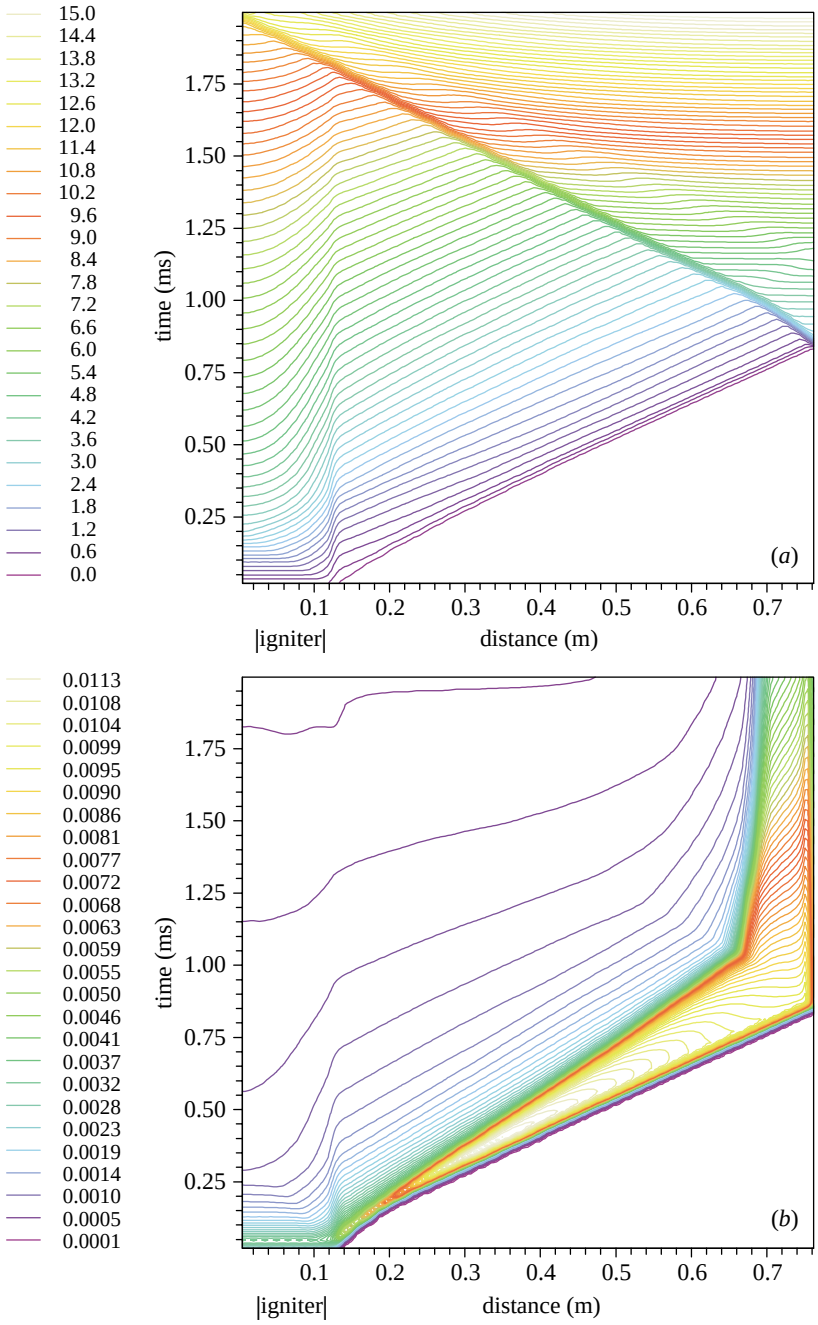

Figure 2. The pressure (a) and mass fraction (b) in the combustion chamber over the first 2 ms.

and source terms may be handled separately. It is then apparent that the solid-phase flow equations completely decouple from the gas-phase equations and so they can be solved independently from the gas-phase flow equations. The solution procedure

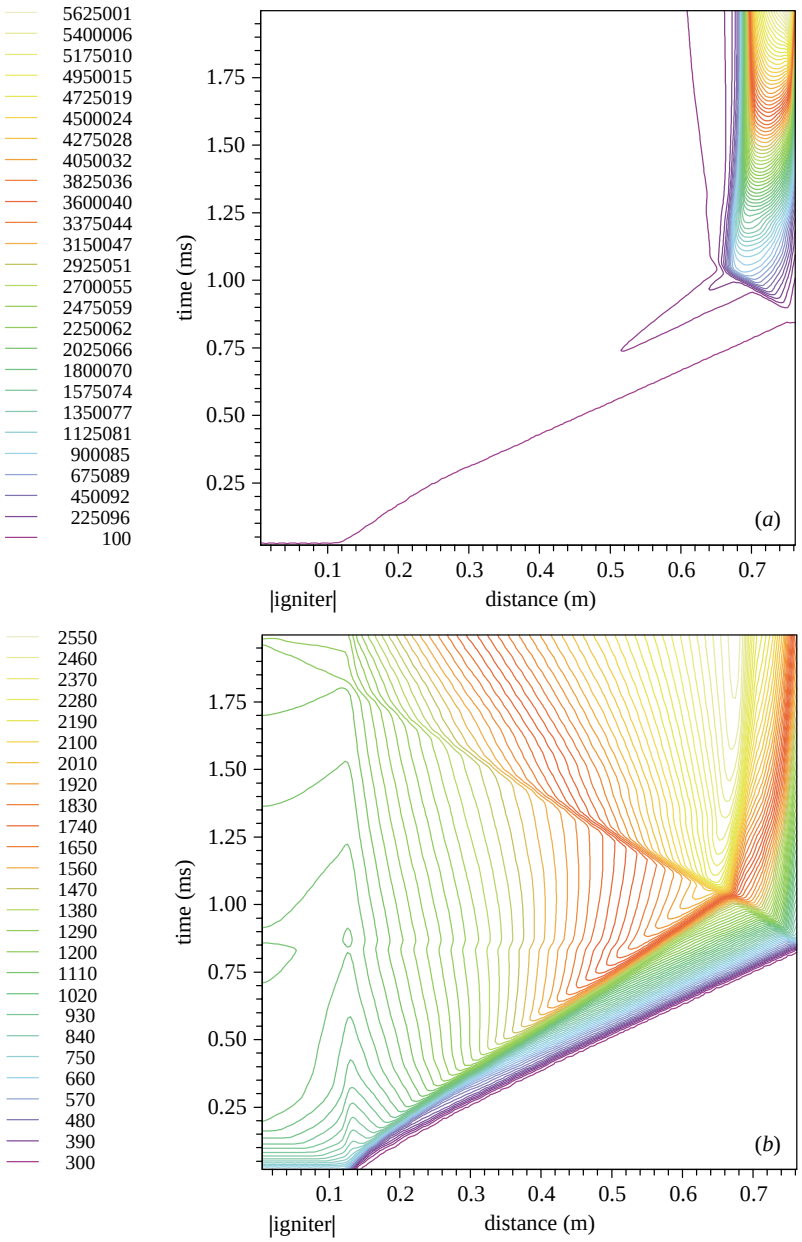

Figure 3. The reaction rate (a) and temperature (b) in the combustion chamber over the first 2 ms.

then involves individual hyperbolic problems for the gas phase and the solid phase, followed by the solution of a system of ordinary differential equations that takes into account the source terms $\boldsymbol{S}(\boldsymbol{U})$. The hyperbolic problems are given as

$$(\boldsymbol{U}_{\mathrm{g}})_t + \boldsymbol{F}(\boldsymbol{U}_{\mathrm{g}})_x = 0, \quad (\boldsymbol{U}_{\mathrm{p}})_t + \boldsymbol{F}(\boldsymbol{U}_{\mathrm{p}})_x = 0. \tag{3.3}$$

Each is solved using a shock-capturing finite-volume scheme, the weighted-average-flux scheme (WAF) (Toro 1989*b*). This is a second-order extension of Godunov's method and requires the solution to the Riemann problem between adjacent cells of the spatial domain. An approximate solution to the Riemann problem—the HLLC method (Toro *et al*. 1994)—is adopted. This is entirely for reasons of efficiency since the solution of the gas-phase Riemann problem with a covolume equation of state necessitates extensive use of iterative methods to construct an exact solution. The HLLC method constructs the solution by calculating estimates of the wave speeds from the initial conditions. These are formulated in an adaptive manner for both gas-phase and solid-phase Riemann problems depending on the difference in the initial values (details can be found in Lowe (1996)).

Finally, the system of ordinary differential equations is given as

$$(\boldsymbol{U}_{\mathrm{g}})_t = \boldsymbol{S}(\boldsymbol{U}_{\mathrm{g}}), \quad (\boldsymbol{U}_{\mathrm{p}})_t = \boldsymbol{S}(\boldsymbol{U}_{\mathrm{p}}). \tag{3.4}$$

These are solved together using a stiff-solver package (Hindmarsh 1980) that can readily deal with the relatively short time-scales associated with chemical kinetics.

4. Ignition simulation

This first simulation is on a test problem over the early stages of combustion. The chamber is as illustrated in figure 1. Igniter gas is vented over the first sixth of the chamber. The projectile base remains fixed due to the low pressures throughout this period.

Figure 2 illustrates flow-variable histories over the first 2 ms in the combustion chamber. The igniter flux distribution causes the temperature over the first sixth of the chamber to increase. This promotes the formation of a compression wave that travels towards the far end of the chamber and reflects, which can be seen as the straight-line feature on the pressure picture between (0.14 m, 0 ms) and (0.762 m, 0.85 ms). The temperature in the igniter-flux region and behind the compression wave is higher than the gasification temperature (420 K) and so mass fraction is introduced into the chamber as seen from the mass-fraction plot. However, there is also another straight-line feature on the mass-fraction plot that lags behind the compression wave between positions (0.18 m, 0.25 ms) and (0.66 m, 1 ms). This was first identified in previous work (Clarke & Lowe 1996) as the movement of reactant species produced in the hot igniter-flux region and advected into cooler regions, and will be described as a 'reactant wave'. However, while the mass-fraction plot can display the change in reactant concentration within the chamber, a more important quantity is the reaction rate distribution. This relationship, dependent on species concentration and temperature, controls the rate of energy release in the chamber. Figure 3 displays the reaction rate and temperature in the chamber. The absence of curves at early times in figure 3*a* indicates how the reaction rates are much higher in the region defined between points (0.762 m, 0.75 ms), (0.66 m, 1 ms) and the line $x = 0.66$ m. The point (0.66 m, 1 ms) is significant for it defines the position at which the reflected shock and the reactant wave intersect. This provides a combination of high concentration of reactant species and high temperature, consequently producing higher reaction rates.

Finally, figures 4 and 5 describe profiles of solid-particle motion in the chamber. Figure 4 illustrates both particle velocity and porosity distribution at times 0.5, 0.75

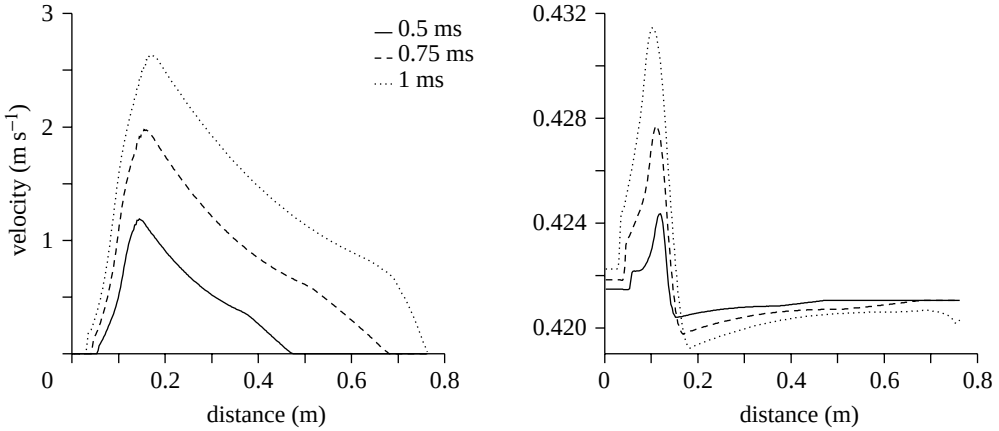

Figure 4. Particle velocity and porosity profiles at 0.5, 0.75 and 1 ms.

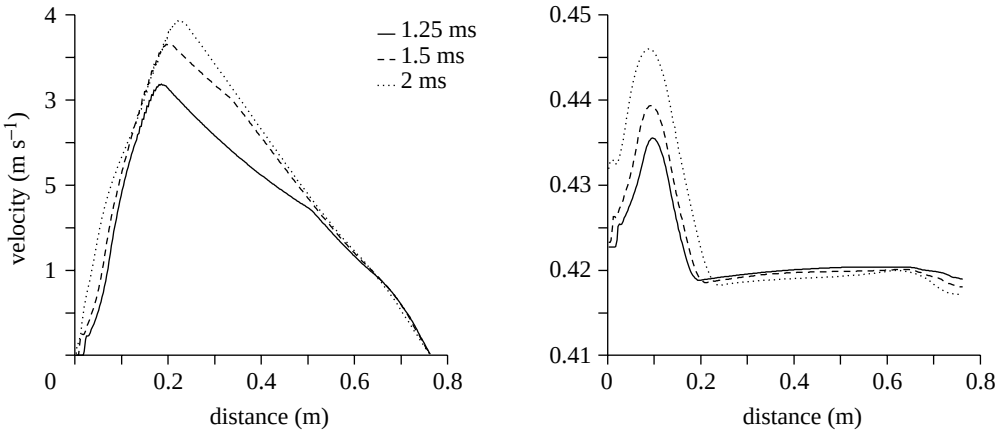

Figure 5. Particle velocity and porosity profiles at 1.25, 1.5 and 2 ms.

and 1 ms. Throughout these times the solid is accelerating, at a relatively low speed, away from the primer region, dragged by the gas which is moving at a higher velocity towards the far end of the chamber. This creates a dense region of solid around the end of the primer tube and sparser density of solid at the primer. Figure 5 represents the motion at times 1.25, 1.5 and 2 ms. At these times, from figure 2, the reflected shock is such that the gas velocity is negative and moving towards the primer end. However, figure 5 shows how the particles are still moving in the opposite direction and the effect of drag, at these times, is only sufficient to decelerate the motion, recognized from the fact that the velocity profiles are getting closer together.

The above findings are counter-intuitive; a brief glance at the chamber configuration might immediately lead to the conclusion that the primer will create higher temperatures and pressures at this end of the chamber. However, the inclusion of chemical kinetics immediately reveals that the highest rates of reaction occur at the far end of the chamber. Further, the modelling of solid-particle motion also contradicts this since the primer configuration assists movement of particles away from the region. Since the bulk of the energy released in the chamber is due to the propellant,

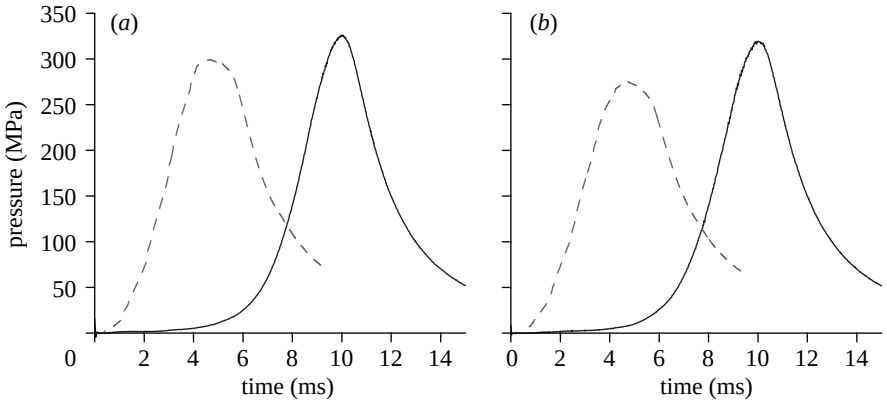

Figure 6. Pressure distribution at locations one (a) and three (b): experiment (—) and equilibrium simulation (- - -).

and not the small amount of energy from the igniter powder, the lower density along the primer may eventually mean lower temperatures and pressures.

5. Test problem

The ballistic problem will be investigated, where the incentive is to predict the pressure at the projectile base so that the force on the projectile can be calculated. From this information the velocity and time at which the projectile leaves the muzzle can be deduced. Experimental data† give the pressure at three different axial locations along the axial length—one reading, which will be denoted as location one, is close to the breech, the second is centrally located in the chamber and the third, location three, is close to the initial projectile position. Figure 6 shows pressure plots at locations one and three where experimental data are given by the solid line. The experiment displays a 2 ms delay prior to any noticeable pressure increase. Between times 2 ms and 6 ms there is a gradual increase in pressure from 0.1 to 25 MPa. Finally, between 6 ms and 10 ms, the rate of pressure rise increases to an almost constant value until it attains a maximum pressure of 330 MPa.

The dashed lines in figure 6 describe numerical simulations based on the equilibrium two-phase equations. A gas-temperature ignition criterion has been used where $T_{\mathrm{ig}} = 435$ K. This very simple attempt at modelling ignition predicts a delay of only 0.35 ms. Further, the rate of rise in pressure after ignition is much higher than in the experiment. From this it is fair to say that the equilibrium model inadequately captures both ignition delay and the early stages of combustion. Along with this the peak pressure is lower than the experimental prediction by almost 30 MPa.

Figure 7 compares the numerical simulation with a one-step gas-phase reaction and experiment (where $E_{\mathrm{A}}/R = 500$ K, $A_{\mathrm{g}} = 0.000\,15$). The ignition delay of the simulation is now greater than experiment. The increase in delay from 0.35 ms to 5 ms is attributed to the measurable time delay between first gasification and gas-phase reaction not permissible in the equilibrium solution. The shift in time produces much better agreement in the time at which the pressure peaks. However, despite this agreement comparison of the simulation and the experiment still displays marked

† Courtesy of the Defence Evaluation and Research Agency, Fort Halstead.

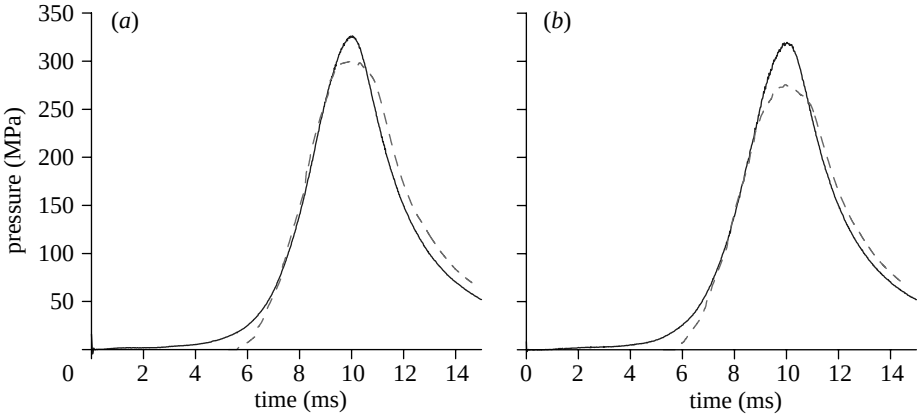

Figure 7. Pressure distribution at locations one (*a*) and three (*b*): experiment (—); one-step non-equilibrium simulation (- - -).

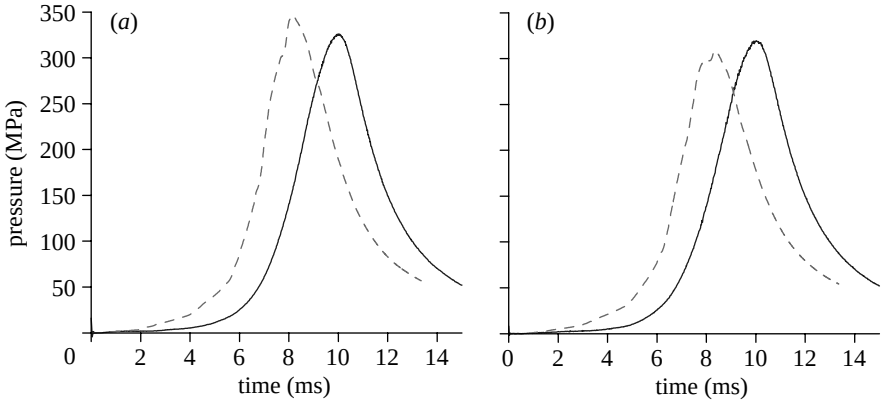

Figure 8. Pressure distribution at locations one (*a*) and three (*b*): experiment (—); two-step non-equilibrium simulation (- - -).

differences—in fact this curve merely looks like the equilibrium curve displaced in time by 5 ms and the rate of rise in pressure at early times and peak pressures is still inaccurate.

Now compare these solutions with a two-step reaction scheme, described in figure 8. In this simulation the first step will be assumed to take place infinitely fast and so energy released due to the first reaction, Q_{R}, is released instantly on gasification. $Q_{\mathrm{R}} \approx 20\%$ of the total chemical energy of the propellant. This energy release is now responsible for the gradual increase in energy at early times. At 4.5 ms the second reaction takes place (where $E_{\mathrm{A}}/R = 1200\,\mathrm{K}$ and $A_{\mathrm{g}} = 0.000\,04$), releasing the larger proportion of energy Q_{g} (80% of the total solid chemical energy) into the chamber. The combination of slow energy release followed by more rapid energy release produces a substantially higher peak pressure that could not be produced using either of the previous models.

The general form of the curve provides a closer fit to the experimental data; however, ignition still occurs (about) 1.5 ms earlier than seen in the experiment. Close scrutiny of the experimental pressure curves indicates that the pressure in the cham-

ber does not change over the first 2 ms. The model above *assumes* that the solid surface decomposes when the gas-temperature reaches *ca.* 420 K. This corresponds with first energy release produced by the first chemical reaction and the pressure slowly increases. It is apparent that this initial rise in pressure is occurring 1.5 ms too early.

The first possible explanation is that the solid does not actually gasify at 420 K and it takes 2 ms before heat transfer, between the gas and solid, produces any gasification of the propellant. Many early theories (see, for example, Hermance 1984) concentrate on modelling this part of the ignition cycle. In these works, distinct periods of 'inert' heating followed by surface reaction have been identified, prior to ignition. A simple model of these heat-transfer processes has not been included here but details can be found in Lowe (1996).

Secondly, as mentioned previously, the first chemical reaction has been assumed to occur at an infinitely fast rate; if this were not so then the time between first gasification and the energy release from this reaction could explain the 1.5 ms time delay.

6. Conclusions

Gas-phase chemical kinetics have been included into internal ballistic models and the effect on burning and ignition explored. The investigation indicates that non-equilibrium effects can be used to describe the pressure histories more accurately during the early stages where the equilibrium models are inaccurate. The single-step chemical scheme can improve modelling of ignition by providing a rational understanding of why first gasification can occur prior to ignition and why ignition is often observed away from the primer stimuli. However, after ignition the general rate in change of pressure will be identical to the equilibrium model. The two-step chemical model retains all the attributes of the one-step model and also provides an explanation for the gradual increase in pressure at early times that can be seen in experiment. By adopting this idea much higher peak pressures can also be predicted.

We thank the WX6 department of the Defence Evaluation and Research Agency (DERA) at Fort Halstead, UK, who sponsored the work and provided valuable experimental data (British Crown Copyright 1997/DERA).

References

Clarke, J. F. & Lowe, C. A. 1996 Combustion with source flows. *Math. Computer Modelling* **24**, 95–104.

Great Britain Ministry of Supply Scientific Advisory Council 1951 *Internal ballistics*. HMSO.

Drew, D. A. 1983 Mathematical modelling of two-phase flow. *Ann. Rev. Fluid Mech.* **15**, 261–291.

Gough, P. S. 1974 The flow of a compressible gas through an aggregate of mobile reacting particles. PhD thesis, McGill University, Department of Mechanical Engineering.

Hermance, C. E. 1984 Solid propellant ignition theories and experiments. *Progress in Astronautics and Aeronautics*, vol. 90, pp. 241–289. AIAA.

Hindmarsh, A. C. 1980 Two new initial value ordinary differential equation solvers. *ACM SIGNUM Newsletter* **15**, 10–11.

Lowe, C. A. 1996 CFD modelling of solid propellant ignition. PhD thesis, Cranfield University Press.

Lowe, C. A., Toro, E. F. & Clarke, J. F. 1995 Numerical methods for propellant systems. In *1st Asian Computational Fluid Dynamics Conf., Hong Kong University of Science and Technology, Clearwater Bay, Hong Kong*, pp. 541–549.

Peretz, A., Kuo, K. K., Caveny, L. H. & Summerfield, M. 1973 Starting transient of solid propellant rocket motors with high internal gas velocities. *AIAA Jl* **11**, 1719–1727.

Ransom, V. H. & Hicks, D. L. 1984 Hyperbolic two-pressure models for two-phase flow. *J. Comput. Phys.* **53**, 124–151.

Smirnov, N. N. & Dimitrenko, I. D. 1992 Convective combustion of porous compressible propellants. *Combust. Flame* **89**, 260–270.

Soo, S. L. 1979 Equation of motion of a solid sphere suspended in a fluid. *J. Multiphase Flows* **18**, 263–264.

Toro, E. F. 1989*a* The WAFBC1 internal ballistic manual. Report, Aerodynamics Department, Cranfield Institute of Technology.

Toro, E. F. 1989*b* A weighted average flux method for hyperbolic conservation laws. *Proc. R. Soc. Lond.* A **423**, 401–418.

Toro, E. F., Spruce, M. & Speares, W. 1994 Restoration of the contact surface in the HLL solver. *Shock Waves* **4**, 25–34.

Yanenko, N. 1977 *The method of fractional steps*. Springer.